An Electro-Optic Direction Sensor

ALAN R. JOHNSTON*
Jet Propulsion Laboratory, California Institute of Technology, Pasadena, Calif.

A single-axis star sensor is described in which a wave plate having direction-dependent retardation, together with an electro-optic modulator, provides the basis for indicating the direction of a distant point source of light. An alternating current photosignal is obtained, thus avoiding problems associated with detector drift. An analysis of the nominal sensor performance is compared with measurement and found to be in good agreement. The effect of varying the optical geometry on field of view is calculated. The effective noise input is evaluated. Satisfactory tracking of a + 1 magnitude star with a 1 cm aperture and a photomultiplier detector was demonstrated, showing a signal-to-noise ratio of about 50 on an rms basis.

Introduction

A NEW type of star sensor, called an "electro-optic direction sensor," will be described in this paper. It is a device which generates an angular error signal useful for pointing an instrument or for attitude control of a spacecraft by sensing a distant light source such as a star. The sensor is inherently a single-axis device—i.e., it senses an angle in one plane, while its output is independent of angle in the perpendicular direction. Two such devices would be used for pointing an instrument toward a beacon, but one would suffice for roll-axis stabilization of a spacecraft about the sun line. The basic phenomenon on which the sensor depends is the direction-dependent birefringence of an optically anisotropic crystal. No moving parts are involved. An electro-optic modulator permits operation of the detector itself in an a.c. mode, thus avoiding effects from dark-current drift or low-frequency detector noise. A simple detector such as a photomultiplier or low-noise, solid-state detector suffices, as $X - Y$ outputs are not needed.

In the past, three identifiable methods of optical direction sensing have been used frequently and, of course, many variations also exist.[1] Background material on celestial star trackers is given in Ref. 2, and a bibliography is available in Ref. 3. Arrays of detectors can be arranged in the image plane of a lens in such a way that the directional information is obtained by noting which detectors are illuminated.[4, 5] Alternatively, various mechanizations in which the image is either scanned or nutated over a detector have been constructed, usually with a mirror or counter rotating prisms. Mechanical chopping by means of rotating or vibrating elements has also been used[6] rather than scanning. Finally, a technique may be employed in which image scanning is done with electron optics using an image-dissector tube or vidicon.[7] The image-dissector approach has been developed to a very sophisticated state for roll-attitude stabilization of Mariner-type spacecraft about the sun line.[8] In all three approaches, the operation which yields the directional information occurs in the image plane. On the other hand, the essential sensing operation takes place in the entrance aperture instead of in the image plane of the device described in this paper.

Although the three methods mentioned have been successfully applied, it is felt that our device has potential advantages that may be of value in future applications. It would offer an alternative no-moving-parts approach that is independent of the relatively complex and expensive image-dissector tube. It is also relatively simple and compact, and therefore promises good reliability and low weight.

In the following sections, the optical and electronic configuration of the sensor will be described, and the principle of its operation will be explained qualitatively. The behavior of the important optical elements is then analyzed in detail. The results, given in graphical form, would be useful for sizing the optical elements for a given task, and also for calculating the expected output signal. Next, the calculated parameters are compared with experiment for a specific set of optics which were set up on an optical bench. The expected noise behavior of the sensor is then calculated from detector noise-effective power (NEP) figures. The entrance aperture required for a given star intensity, response time, and noise level is estimated and compared with some initial noise data.

Description of the Device

A pictorial diagram of the sensor optics is shown in Fig. 1. The optics can be divided into two main parts: a sandwich of birefringent optics, called a "direction-sensitive modulator," and a set of conventional telescopic optics which collects the light, directs it onto a detector, and also defines a field of view. Since the function of the telescope is straightforward, it will not be discussed further. The direction-sensitive modulator consists of five elements: a polarizer, directional wave plate (DWP), compensator, modulator, and analyzer. Optically, the DWP and compensator are both fixed retarders (optical phase shifters), whereas the modulator acts as a time-varying retarder. A more complete discussion of the anisotropic optics of crystals is contained in a text by E. A. Wood.[9] These elements are illustrated again in Fig. 2, but separated in order to show the optic axis and orientation of each element. The coordinate system shown, with Z along the nominal axis of the sensor, will be used throughout this discussion.

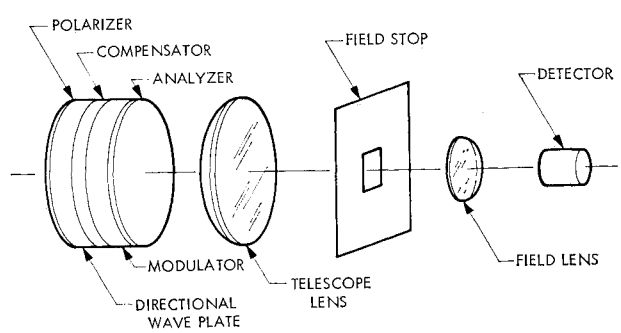

Fig. 1 Pictorial diagram of the sensor.

Received June 28, 1971; presented as Paper 71-966 at the AIAA Guidance, Control and Flight Mechanics Conference, Hempstead, N.Y., Aug. 16-18, 1971; revision received May 8, 1972. This paper presents the results of one phase of research carried out at the Jet Propulsion Laboratory, California Institute of Technology, under Contract NAS 7-100, sponsored by NASA.

Index category: Spacecraft Attitude Dynamics and Control.

* Member of the Technical Staff.

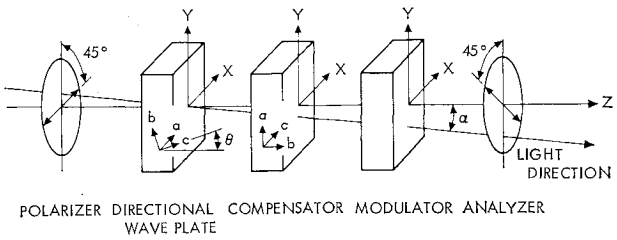

Fig. 2 Diagram of the direction-sensitive modulator, showing the orientation of each component.

The directional wave plate is cut from an optically uniaxial material, such as quartz or calcite, so that the optic axis forms an angle θ with the normal to its faces. It is oriented normal to Z and rotated about Z so that the projection of its optic axis on its surface is parallel to Y. Aligned thus, the birefringent axes of the wafer coincide with X and Y. For near-axial rays, its retardation will depend linearly on the direction of propagation of the light in the $Y-Z$ plane. The inclination of a ray from the Z direction is specified by α in Fig. 2. The compensator is made from the same material as the DWP, but is cut with its optic axis parallel to its surfaces and oriented with its axis along X. Its function is to compensate the large birefringence of the DWP for light traveling parallel to the instrumental axis ($\alpha = 0$), and even more importantly, it compensates the dispersion in retardation so that the device will function in white light.

The modulator, following the DWP and compensator in the figure is oriented such that its induced axes of birefringence are aligned along X and Y. It superimposes a sinusoidally varying (with time, not direction) retardation on the direction-dependent retardation of the wave plates. It is desirable for the modulating element to be isotropic when not being driven in order to avoid distortion of the desired dependence of the total retardation on direction. Unfortunately, this is not the case for potassium dihydrogen phosphate (KDP), the most convenient modulator material, and a field-of-view limitation (to be discussed later) results. The crossed polarizer and analyzer, at 45° to Y, convert the total modulated retardation into an intensity which can be detected and processed electronically.

Taken as a whole, the direction-sensitive modulator behaves like a filter in which the transmission depends on the direction the light travels through it.

A quantitative analysis of the sensor will be made in the next section of this paper, but its function can be qualitatively described in the following way. The directional wave plate and compensator, when placed between crossed polaroids, will exhibit a set of, let us say, horizontal fringes on a distant screen if floodlighted from the opposite side. This pattern of fringes corresponds to the interference figure of a crystal as displayed by a polarizing microscope, and in fact is the interference figure of the direction-sensitive modulator.[9] If the screen is far enough away, a position on the screen will correspond to a specific direction of incidence. When the electro-optic modulator is energized, it wobbles the entire fringe pattern in the vertical direction with frequency ω. The substitution of a distant point source such as a star for the floodlight can be modeled by putting a small hole at the appropriate point in the screen and detecting only the light passing through the hole. The amount of light passing through will be modulated as the fringes move up and down, with phase and amplitude depending on the position of the hole with respect to the unmodulated fringe position. The resulting photosignal is converted to a slowly varying dc error signal by means of a phase-sensitive detector.

A block diagram of the sensor electronics is shown in Fig. 3. The preamplifier is matched to the detector and should be optimized to bring the signal above the noise level of the following electronics in the most expeditious way. The phase-detector reference is supplied from the modulator driver so that the signal component containing the directional information is extracted from the photodetector output at frequency ω. The phase-sensitive detector also provides filtering, which determines the information bandwidth of the device.

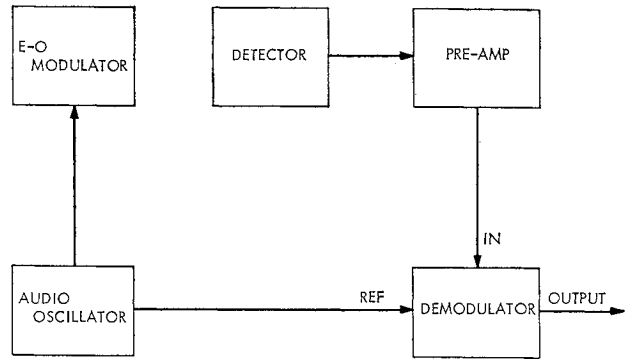

Fig. 3 Block diagram of the sensor electronics.

Analysis

In this section, expressions are derived for the useful angular field of the sensor, for the transfer function between direction and the sensor output, and for the magnitude of the second harmonic component of the photosignal. The latter is potentially useful as an acquisition signal to verify the presence of the light source in the field of view. Both DWP and compensator are assumed to be plane-parallel slices of thickness t_w and t_c, respectively, of the same optically uniaxial material. The geometry has already been given in Fig. 2. An incident light beam from a distant point source is assumed. The direction of propagation of this plane wave is specified by a unit vector $\bar{S}$ along the wave normal.

$$\bar{S} = S_x, S_y, S_z \tag{1}$$

Consider first the directional wave plate. Its crystallographic axes are the system a, b, c, with c in the $Y-Z$ plane at an angle θ to Z. In general, the angle θ is not small. The orientation of the identical a and b axes is not important, but for convenience we arbitrarily choose a along X.

In the crystal, the extraordinary index (E vector of light in the $Y-Z$ plane) will depend on the angle between the wave normal and c. Accordingly, the direction of the wave normal within the crystal must be found with respect to the a, b, c coordinates in terms of the direction $\bar{S}$ of the incident light. Inside the wave plate, the wave normal is bent toward the Z axis, resulting in a new propagation vector $\bar{S}'$

$$\bar{S}' = S_x', S_y', S_z' \tag{2}$$

Assuming that the ray is nearly parallel to Z, $S_x \approx S_y \approx S_z$, and

$$S_x' = S_x/n_e;\ S_y' = S_y/n_e \tag{3}$$

Similarly, the components of $\bar{S}'$ can be given, with respect to the crystal system, as

$$\bar{S}' = p, q, r \tag{4}$$

The components p, q, r can be obtained from S_x', S_y', S_z' by means of a coordinate rotation, with the result that

$$r = S_y' \sin\theta + S_z' \cos\theta \tag{5}$$

The phase velocity v_p for a wave with e polarization and wave normal at an angle ψ to the c axis ($\cos\psi = r$) is given by Born and Wolf[10] as

$$v_p^2 = v_o^2 \cos^2\psi + v_e^2 \sin^2\psi \tag{6}$$

where v_o and v_e are the two principal propagation velocities: $v_o = c/n_o$, and $v_e = c/n_e$. From (6) we can obtain an effective index $n = c/v_p$,

$$n^2 = \frac{n_e^2}{1 + r^2[(n_e^2 - n_0^2)/n_0^2]} \tag{7}$$

The optical path for the e ray, measured in radians, is

$$\Gamma_e = 2\pi t_w n/\lambda S'_{ze} \tag{8}$$

where t_w is the geometrical thickness of the wave plate, and λ the light wavelength in air. The direction cosine S'_{ze} allows for the slight increase in geometrical thickness caused by the inclination of the light beam. It is included here for completeness, but is not a significant correction since S_x, S_y are assumed small

$$S'_{ze} = [1 - (S_x/n_e)^2 - (S_y/n_e)^2]^{1/2} \tag{9}$$

A similar expression can be written for the ordinary ray by substituting n_o for n_e and noting that the ordinary index does not depend on direction

$$\Gamma_o = 2\pi t_w n_o/\lambda S'_{zo} \tag{10}$$

The retardation of the directional wave plate $\Delta\Gamma$ is the difference

$$\Gamma_e - \Gamma_o = \Delta\Gamma = (2\pi t_w/\lambda)(n/S'_{ze} - n_o/S'_{zo}) \tag{11}$$

In principle, the retardation can be calculated from (11) for any direction of incidence, since n depends on S_y through (3), (5), and (7).

Note that if $\Delta\Gamma$ from (11) is expressed as a power series in S_y, the leading term is linear, as follows:

$$\Delta\Gamma = (\text{constant term}) + 2\pi t_w\, \Delta n \sin^2\theta S_y/\lambda n_o + (\text{higher order terms}) \tag{12}$$

where Δn is the birefringence of the material, defined as $n_e - n_o$. We have assumed small birefringence; that is, $\Delta n \ll n_e$. Note that $\Delta\Gamma$ does not depend on S_x; angles in the X direction are not sensed.

The retardation of the compensator can be obtained in a similar way, by taking into account the different orientation of its a, b, c coordinate system. In the result from the preceding analysis for the DWP, the x and y axes must be interchanged and θ set equal to $\pi/2$. The result is

$$\Delta\Gamma_c = (2\pi t_c/\lambda)(n_o/S'_{zo} - n_e/S'_{ze}) \tag{13}$$

The quantity $\Delta\Gamma_c$ does not contain a linear term in either S_x or S_y because the $\cos\theta$ term in (5) vanishes for $\theta = \pi/2$, so that r in (7) becomes $r = S'_x$. Physically, this means that the retardation of the compensator is nearly independent of the propagation direction for small inclinations. We can therefore conclude that the retardation of the DWP and compensator together will vary linearly with S_y, but will be independent of S_x. Accordingly, S_x can be ignored and the behavior of the device described in terms of a light beam traveling in the $Y-Z$ plane. We will specify the direction of the ray in terms of the angle α it forms with Z ($\sin\alpha = S_y$).

In order to achieve the desired on-axis compensation, we require that the total retardation be zero for an axial ray

$$\Delta\Gamma + \Delta\Gamma_c = 0 \qquad \text{for } \alpha = 0 \tag{14}$$

From (11), (13), and (14), and by making the approximation that $\Delta n \ll n_o$, the following condition on the relative thickness of DWP and compensator can be derived

$$t_c/t_w = \sin^2\theta \tag{15}$$

Eq. (15) states that the ratio of the thicknesses of the DWP and compensator must be properly adjusted for exact on-axis compensation. The condition for compensation is wavelength-independent since it does not contain λ or Δn, a fact which permits the device to function in white light.

Up to this point, the analysis has been concerned with the DWP and compensator only. The retardation introduced by the modulator Γ_m must also be included in order to calculate the modulated light intensity as a function of α. We assume a sinusoidal modulator drive at frequency ω, so

$$\Gamma_m = \Gamma_{mo} \sin\omega t \tag{16}$$

The quantity Γ_{mo} is a modulation index given by

$$\Gamma_{mo} = \pi V_p/V_{\lambda/2} \tag{17}$$

where V_p is the peak value (not peak to peak) of the voltage applied to the modulator, and $V_{\lambda/2}$ is the half-wave voltage of the modulator—namely, the voltage that would be required to obtain 100% modulation with it between crossed polaroids. Figure 4 gives Γ_{mo} in terms of V_p and $V_{\lambda/2}$.

The total retardation of the three elements will be

$$\Delta\Gamma_{tot} = \Delta\Gamma + \Delta\Gamma_c + \Delta\Gamma_m \tag{18}$$

Substituting (11) for $\Delta\Gamma$, (13) for $\Delta\Gamma_c$, (16) for $\Delta\Gamma_m$, and making the approximations appropriate for small birefringence and small α that were obtained earlier, we obtain

$$\Delta\Gamma_{tot} = (2\pi t_w/\lambda)(\Delta n\alpha/n_{av})\sin^2\theta + \Gamma_{mo} \sin\omega t \tag{19}$$

The quantity n_{av} is an average index, and can be taken as either n_o or n_e with small error. In deriving the aforementioned expression (the condition for compensation on-axis, (15) has also been used. This condition by its design has eliminated terms in $\Delta\Gamma_{tot}$ not containing α, with the result that $\Delta\Gamma_{tot}$ must equal zero for $\alpha = 0$ and no modulation.

The analyzer is set at 45°, as shown in Fig. 2, and converts the total retardation into an intensity

$$I = I_o \sin^2(\Delta\Gamma_{tot}/2) \tag{20}$$

Here, I_0 is the intensity of the polarized beam incident on the analyzer, and I is the intensity transmitted to the detector. Defining I_0 after the beam has passed through the polarizer means that the 50% loss inherent in polarizing an incoherent beam must be taken into account by including it in the transmission factor for the optics. The transmission must be defined as the fraction of the intensity passed with polarizer

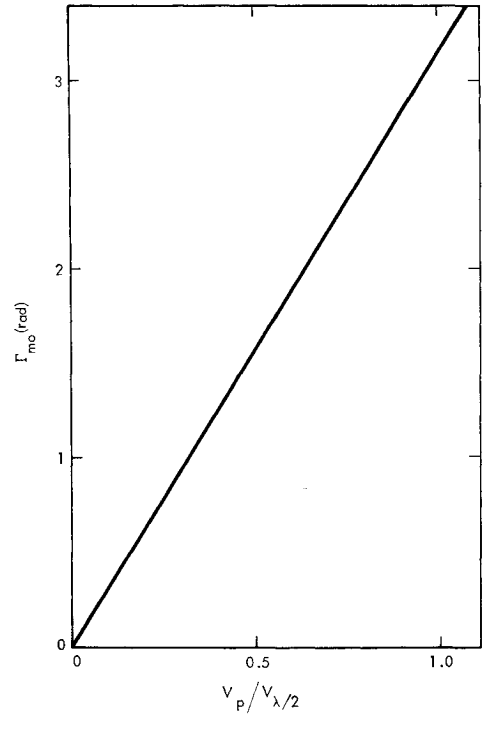

Fig. 4 Modulation index Γ_{mo} vs modulator drive voltage V_p.

and analyzer parallel, instead of crossed for an axial beam $\Delta\Gamma_{tot} = 0$.

Rewriting (20), we obtain

$$I = I_0/2\{1 - \cos[(\pi/2)\alpha/\alpha_{max} - \Gamma_{mo}\sin\omega t]\} \quad (21)$$

where a number of constants have been grouped into an angular scale factor α_{max}

$$\alpha_{max} = \lambda n_{av}/4t_w\,\Delta n\sin^2\theta \quad (22)$$

Thus, α_{max} depends on the wave plate material and thickness. Eq. (21) can be expanded to

$$\frac{I}{I_0} = \frac{1}{2} - \frac{1}{2}\cos\left(\frac{\pi}{2}\frac{\alpha}{\alpha_{max}}\right)J_0(\Gamma_{mo}) - \sin\left(\frac{\pi}{2}\frac{\alpha}{\alpha_{max}}\right)J_1(\Gamma_{mo})\sin\omega t$$
$$- \cos\left(\frac{\pi}{2}\frac{\alpha}{\alpha_{max}}\right)J_2(\Gamma_{mo})\cos 2\omega t + \text{higher harmonics} \quad (23)$$

where J_i are the Bessel functions of order i.

Thus the transmitted intensity has a component at frequency ω which varies as $\sin A\alpha$, where $A = \pi/2\alpha_{max}$, which can be isolated by a phase-sensitive detector using the modulator drive as a reference. If $|\alpha| \gtrsim \frac{3}{4}\alpha$ max, one can operate the quasi-linear part of the sinusoidal curve; but if $\alpha > \alpha$max, the output will decrease again. Accordingly, α_{max} will be considered the useful field of view, and the telescopic optics should be made to accept a field roughly $2\alpha_{max}$ wide—i.e., $-\alpha_{max} < \alpha < \alpha_{max}$. The useful field of view in the X direction, perpendicular to the sensitive axis of the sensor, is not similarly restricted, and could be set many times larger than α_{max} if desired.

Figure 5 is a plot made from Eq. (22) showing the dependence of the useful field of view α_{max} on DWP thickness for three materials of widely differing birefringence: quartz, KDP, and calcite, with $\theta = 45°$.

Figure 6 gives the magnitude of the fundamental component of the transmitted intensity $(I/I_0)^{\omega}$ as a function of α and the parameters α_{max} and Γ_{mo}. This quantity is proportional to the output signal available from the phase detector.

Figure 6 shows that the optimum value of Γ_{mo} is 1.8, corresponding to a V_p of approximately half of $V_{\lambda/2}$. However, the modulator could be operated at 50% of optimum drive ($\Gamma_{mo} = 0.9$) with a signal loss of less than 30%.

As mentioned before, the component of transmitted intensity at 2ω, $(I/I_0)^{2\omega}$, could be detected with a tuned preamplifier and used as an acquisition signal. Figure 7 is a

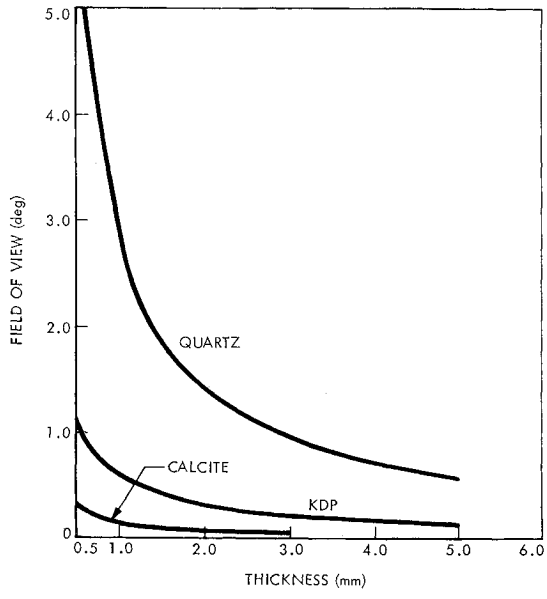

Fig. 5 Field of view as a function of DWP thickness.

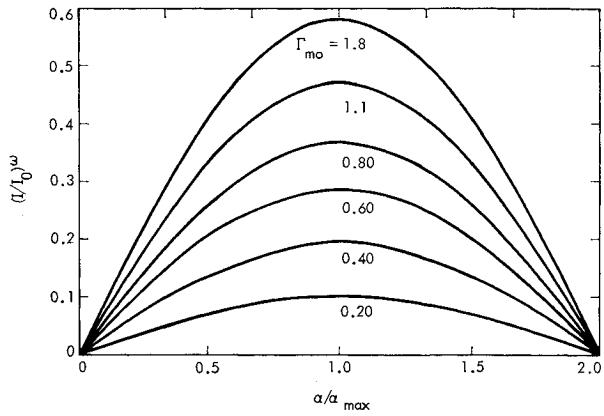

Fig. 6 The component of transmitted intensity at frequency ω as a function of α/α_{max}.

plot showing the magnitude of this signal in terms of Γ_{mo}, α_{max}, and α. The quantity $(I/I_0)^{2\omega}$ is a maximum at $\alpha = 0$ and varies little over the central part of the useful field.

Experimental Verification

The feasibility of the concept has been shown in the laboratory with optical bench hardware and a simulated star. The star image was obtained from a pin hole illuminated by a tungsten ribbon lamp and placed at the focus of a 65-cm focal length collimating lens. The intensity of the source was adjusted with neutral-density filters, while other filters were used to approximate the spectral distribution of a 5500°K blackbody.

The experimental hardware was set up as shown in Fig. 1; however, the elements of the direction-sensitive modulator were spaced out along the axis so that they could be separately mounted for convenience in adjusting their orientation. Since the modulator operates in collimated light over a small field of view, this arrangement presents no optical problems. The limiting aperture of the system was the 1-cm-diam wave plate. A number of DWP-compensator pairs of differing thickness and material were fabricated, but all with $\theta = 45°$, and therefore $t_c = \frac{1}{2}t_w$.

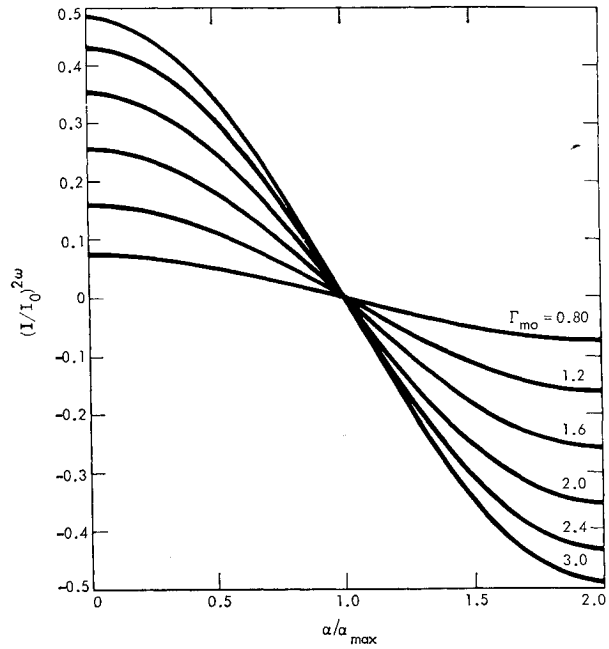

Fig. 7 The component of transmitted intensity at frequency 2ω as a function of α/α_{max}.

The electro-optic modulator was a KD*P (deuterated KDP) wafer 2 mm thick with transparent electrodes (obtained from Crystalab Inc., Rochelle Park, N.J.). Its measured half-wave voltage was 4.4 kv, a value significantly greater than the 3.2 kv expected for KD*P. The reason for the difference is not understood, but may arise from incomplete deuteration.

The polarizer and analyzer were commercial polaroid material (HN-38). The telescope lens was a standard enlarging lens of 100-mm focal length. The detector was an EMI 9536B photomultiplier. No preamplifier was needed, since the phase-sensitive detector was a commercial lock-in amplifier (Princeton Applied Research HR-8).

The magnitude of the photosignal at frequency ω was measured and compared with the $(I/I_0)^\omega$ calculated with the methods of the previous section, using parameters appropriate to the laboratory optics. The DWP for this experiment was of KDP, 2-mm thick with $\theta = 45°$. The modulator was excited with a 500-v peak sinusoidal voltage. The value of I_0, needed in order to find the calculated output, was obtained by turning the analyzer 90° with the simulated star on-axis, and the modulator drive turned off. The d.c. detector signal was then measured to give I_0.

The results are shown in Fig. 8. The nearly linear portion of the output extends roughly to $\alpha = \pm 0.08°$, although a signal indication useful for acquisition would be available out to $\alpha = \pm 0.2°$. The signal at α_{max} is seen to be in close agreement with the calculated value. The calculated α_{max} is somewhat larger than observed, but the difference is reasonable in view of the off-axis birefringence of the modulator, which was neglected in the analysis, and errors in measuring thicknesses.

Figure 9 shows the dependence of signal output on modulator drive voltage at a fixed α for the same experiment. The range of modulator drive voltage shown is low, covering only a portion of the first quarter cycle of $J_1(\Gamma_{mo})$.

Figure 10 is a tracing made with an X-Y plotter, showing data analogous to that in Fig. 8.

This plot was made by scanning the simulated +1 magnitude star at a constant angular rate, while plotting the sensor output as a function of α. The information bandwidth was limited by the lock-in amplifier to a 1-sec time constant, and the aperture was 1 cm in diameter. The figure, showing the observed noise fluctuations, demonstrates that a useful signal-to-noise ratio can be obtained for the bright stars with 1-cm collecting aperture.

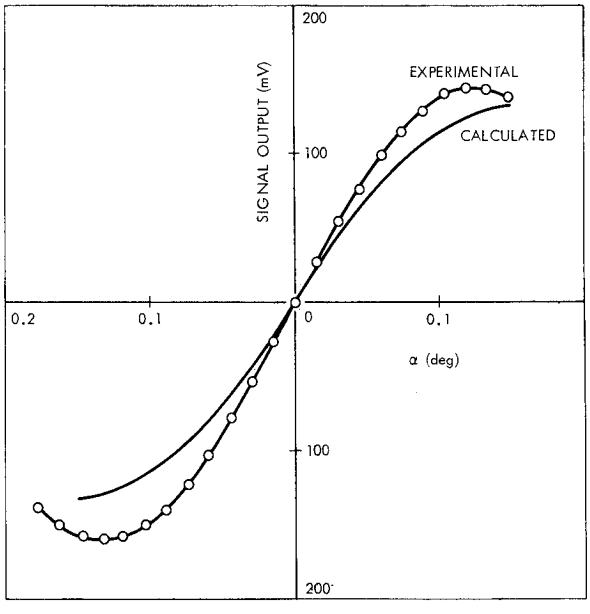

Fig. 8 Experimental sensor output signal compared with the calculated output.

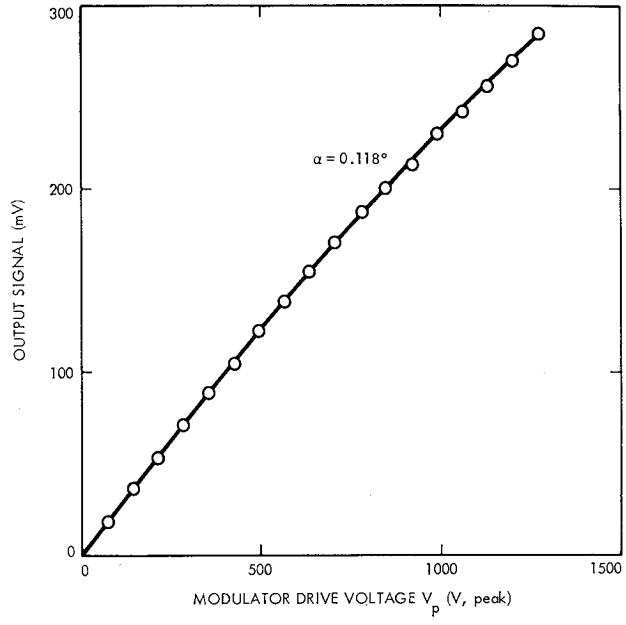

Fig. 9 Experimental sensor output as a function of modulator drive voltage.

Evaluation of the Noise Limitation

The accuracy of pointing toward a dim source, such as a star, is inherently limited by noise, and there is an inverse relationship between pointing accuracy and system-response time. The magnitude of this noise fluctuation is an important constraint in a typical application. An estimate of the equivalent noise input of the present sensor is given below.

There are a number of noise sources, including the noise associated with the electronics, the dark noise from the detector, and the photon noise of the incident light, which is

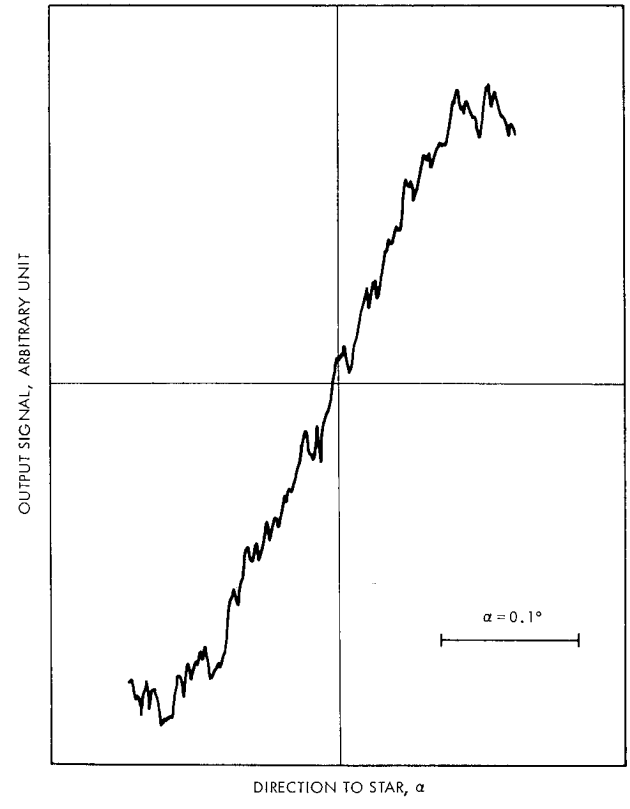

Fig. 10 Experimental output as a function of angle for +1 magnitude star, 1-cm aperture and a photomultiplier detector.

aggravated by the imperfect quantum efficiency of any real detector.

We assume that detector dark noise will dominate, and the following treatment is made in terms of dark noise only. However, for a low-noise photomultiplier, it is possible for photon noise to dominate, requiring modification of the analysis. Our photomultiplier example represents a limiting case, since either reduced dark noise or increased light flux would produce a photon-noise-limited situation.

Let us define a photodetector responsivitity R, a constant which gives the electrical power delivered into the detector load R_L, in terms of the light flux I falling on the detector

$$P = i_{\text{anode}}{}^2 R_L = (RI)^2 \tag{24}$$

The light flux I_i incident on the sensor optics is

$$I_i = M_v A \tag{25}$$

where M_v = the flux from the star in lumens/cm^2, and A is the area of the collecting aperture.

Assume a transmission T for the optics, so that at the detector the maximum available intensity I_0 (analyzer parallel) will be

$$I_0 = M_v A T \tag{26}$$

The (peak) amplitude of the modulated components of the transmitted intensity of the frequency ω is given in terms of this same I_0 by Eq. (23)

$$I^\omega = I_0 \eta \sin[(\pi/2)\alpha/\alpha_{\max}] \tag{27}$$

The quantity η has been introduced for brevity

$$\eta = J_1(\Gamma_{\text{mo}}) \tag{28}$$

The light signal at the detector at ω is then

$$I^\omega = (\pi/2) M_v A T \eta (\alpha/\alpha_{\max}) \tag{29}$$

for α small enough to be on the linear part of the response curve. The rms noise voltage existing at the output of the sensor is calculated from p_n, the noise-effective power of the detector observed under its actual operating conditions and normalized to a 1-Hz bandwidth.

The electrical noise output power of the detector is then

$$P_n = (p_n R)^2 B \tag{30}$$

where B is the signal bandwidth. The noise power at the output of a phase detector is that of the input existing in a band $B = \dfrac{1}{8\tau_1}$, where τ_1 is the time constant of the output circuit of the phase detector, multiplied by the power gain G of the phase detector at its signal frequency[11]

$$P_0{}^{\text{dc}} = G P_{\text{in}}{}^{(\omega)} \tag{31}$$

The $P_0{}^{\text{dc}}$ and $P_{\text{in}}{}^{\omega}$ are, respectively, the output and input electrical powers of the phase detector. Therefore, the noise power at the phase-detector output due to detector dark noise of magnitude p_n would be

$$N = (p_n R)^2 \frac{G}{8\tau_1} \tag{32}$$

The signal power at the phase-detector output is obtained from (24), (29), and (31)

$$S = [(\pi/2)\eta M_v A T R\, \alpha/\alpha_{\max}]^2 G \tag{33}$$

From (32) and (33) an equivalent noise fluctuation $\langle\alpha\rangle_n$ of the input angle α can be obtained

$$\langle\alpha\rangle_n/\alpha_{\max} = 2p_n/\pi\sqrt{8\tau_1}\eta M_v A T \tag{34}$$

The time constant τ_1 is the time constant of the filter in the output circuit of the phase detector. However, a sensor such as this would normally be used as the error sensor in a control loop, and the response time of the closed loop would be expected to be slower than that of the sensor itself. The slower response of the loop averages the noise, and it can be shown that the fluctuation in the closed-loop pointing angle caused by sensor noise is given by the same expression, Eq. (33), with τ_1 replaced by the loop response time. Note that the result calculated from (34) is an rms noise

$$\langle\alpha\rangle_n = (\langle\alpha(t)^2 - \langle\alpha\rangle^2\rangle)^{1/2} \tag{35}$$

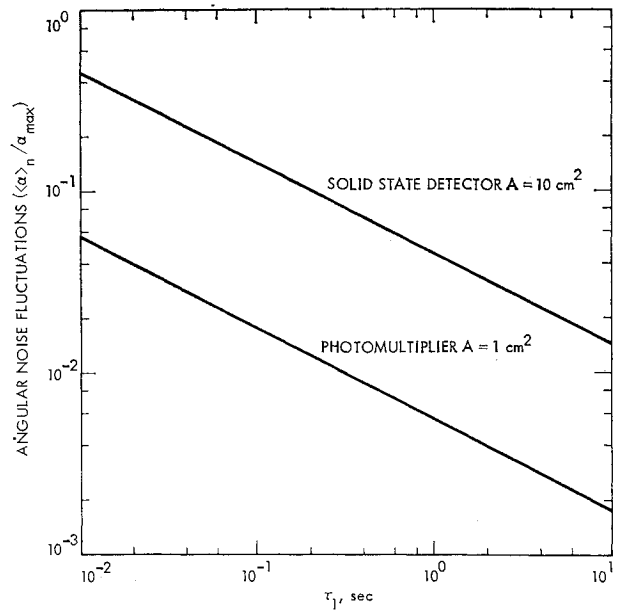

Fig. 11 Calculated noise as a function of response time. Parameters used in the calculation are given in Table 1.

Numerical results are plotted in Fig. 11 for two cases: a photomultiplier detector and a silicon solid-state detector. The significant parameters are given in Table 1. The noise expected for different values of A, p_n, and M_v can easily be obtained by referring to Eq. (34).

The magnitude of the noise observed experimentally and expressed as an equivalent input angular fluctuation was estimated using data of which Fig. 10 represents a sample. The peak-to-peak voltage signal-to-noise ratio observed is approximately 16. The entrance aperture was 1 cm in diameter, the simulated star was +1 magnitude and a 1-sec time constant was used. If the peak-to-peak noise is converted somewhat arbitrarily to rms by dividing it by 3, and appropriate adjustments are made for M_v and A in order to compare it with Fig. 11, an experimental $\langle\alpha\rangle_n/\alpha_{\max} = 0.005$

Table 1 Parameters used in calculating the equivalent noise input of the sensor shown in Fig. 11

Parameter	Photomultiplier detector	Silicon detector
Detector NEP, p_n	4×10^{-13} lumen $Hz^{-1/2}$ (appropriate for 1P21 or 9536B)	3×10^{-11} lumen $Hz^{-1/2}$ (appropriate for HP-4204)
Area of objective A	1 cm^2	10 cm^2
Modulator drive parameter η	0.4	0.4
Transmission of optics T	0.3 (ideal polarizer +60% transmission for remaining optics)	0.3
Incident flux M_v	2×10^{-10} lumen/cm^2 (0 magnitude star)	2×10^{-10} lumen/cm^2

can be estimated. This value falls very close to the photomultiplier curve in Fig. 11, thus confirming the validity of the theoretical noise estimate.

In order to place this calculation in perspective, the equivalent noise input can be estimated for a hypothetical ideal sensor in which the incident energy is partitioned between two photocathodes as a linear function of angle. Only the noise inherently associated with photoemission is considered, the rest of the system being assumed noiseless. The result, taking an incident flux of 2×10^{-10} lumen and a 70 μA/lumen cathode efficiency in order to be comparable to the photomultiplier curve in Fig. 11, would fall a factor of $3\frac{1}{2}$ below it. Thus, the noise of the actual sensor is a factor of $3\frac{1}{2}$ larger than the limit theoretically attainable with a photomultiplier. This factor can be regarded as a measure of the efficiency of the modulation technique employed in the sensor.

Discussion

So far, pointing error and drift have not been treated. A detailed evaluation of this type of error source remains to be done, but we have observed in the laboratory that the null remains stable over a period of several days, at least within the readability of the instrumentation, which was roughly 1% of the angular range α_{max}.

One possible error source whose size can be estimated analytically is the effect of temperature changes on the wave plates. Temperature change to the modulator element does not affect the null. The refractive index and birefringence of all materials depend slightly on temperature, a dependence that will result in a small change in the retardation of each plate. No effect on the null position is expected from simultaneous change in the temperature of both DWP and compensator. A temperature difference between the two elements will cause a shift, however. The magnitude of this shift can be estimated for a pair of quartz plates because the temperature coefficient of the refractive indices is available.[12] The result is $d(\alpha/\alpha_{max})/dT \approx 10^{-5}/°C$, which does not appear to be a serious problem.

The most significant error source is likely to be the presence of unwanted light sources, such as a field of very dim stars or a lighted background within the sensitive field of view, in addition to the desired star or beacon. The concept assumes that there is only one point source present in the sensitive field of view; if there are more than one, their inputs will be averaged. The laboratory model was found to be very insensitive to scattered light—i.e., to light scattered into the detector from sources outside the field defined by the telescope.

A practical constraint on the sensor field of view, as opposed to a null drift, arises from off-axis retardation of the modulator. KD*P appears to be the best choice of material because of its availability in reasonably large size with good optical quality. The modulator crystal is operated with its optic axis along Z in Fig. 2. Therefore, off-axis rays suffer retardation, and distortion of the idealized sensor output occurs. In principle, it would be possible to take into account the effect of the modulator crystal in calculating the sensor output as a function in both X and Y directions. As an example, the null line ($\Delta\Gamma_{tot} = 0$) might be mapped out in two dimensions. Although straightforward, the calculation is complex and would have to be done numerically on a computer.

An angular field of view is often quoted for a KDP-type modulator and typically may be of the order of $\frac{1}{2}$–2°, depending on thickness. This angle is not always defined in the same manner, but one such definition sets the field of view at the angle where the static retardation of the crystal causes a 1% light leak between crossed polaroids. If $\sin^2(\Gamma/2) \approx 0.01$, then $\Gamma \approx 0.2$. The equality $\alpha = \alpha_{max}$ occurs at $\Gamma_{tot} = \pi/2 \approx 1.6$. Therefore, operation within the modulator angular field would result in a maximum distortion of the sensor response of about 12%. The distortion is constant, fixed in time. A reasonable limit on the sensor range is therefore set by the 1% modulator field of view for a KDP-type modulator. A considerably larger field could be available for acquisition, as mentioned before.

In summary, feasibility has been demonstrated for a new type of star tracker which relies on crystalline anisotropy in an oriented waveplate for its ability to sense direction. Its efficiency is such that useful performance can be obtained on the brighter stars with optics of 1–10 cm aperture. It has the advantages of simplicity and no moving parts, and the photodetector operates in an a.c. mode. A specific configuration has been analyzed and tested in the laboratory; however, further detailed work remains to be done in order to fully evaluate its characteristics and limitations.

Possible applications of the new sensor include spacecraft attitude control using a star reference, and pointing of a platform or other gimbaled instrument toward either a natural source or an artificial beacon. The source can be white light. By modifying the signal processing somewhat, the device can also be configured to sense a horizon—i.e., the edge of a lighted area—instead of a point source.

References

[1] Hatcher, N. M., "Spacecraft Attitude Sensors—Where We Stand Today," *Astronautics and Aeronautics*, Vol. 4, No. 12, Dec. 1966, pp. 58–67.

[2] *Celestial Tracker Issue, IEEE Transactions on Aerospace and Navigational Electronics*, Vol. 10, No. 3, 1963.

[3] *Spacecraft Star Trackers*, NASA SP 8026, July 1970.

[4] Koso, D. A. and Kolladge, J. C., "Solar Attitude Reference Sensors," *Proceedings of the Symposium on Spacecraft Attitude Determination*," Rept. TR-0066-(5306)-12, Vol. 1, Oct. 1969, Aerospace Corp., El Segundo, Calif., p. 155.

[5] Astheimer, R. W., "Instrumentation for Infrared Horizon Sensing," *Proceedings of the Symposium on Spacecraft Attitude Determination*," Rept. TR-0066-(5306)-12, Vol. 1, Oct. 1969, Aerospace Corp., El Segundo, Calif., p. 169.

[6] Lansing, J. C., Jr., "Calibration and Spaceborne Performance of the Surveyor Spacecraft Star Sensor," *Journal of Spacecraft and Rockets*, Vol. 5, No. 1, Jan. 1968, pp. 84–89.

[7] Birnbaum, M. M. and Salomon, P. M., "Strapdown Star Tracker for Space Vehicle Attitude Control," *Journal of Spacecraft and Rockets*, Vol. 5, No. 10, Oct. 1968, pp. 1188–1192.

[8] Goss, W. C., "The Mariner Spacecraft Star Sensors," *Applied Optics*, Vol. 9, No. 5, May 1970, pp. 1056–1067.

[9] Wood, E. A., *Crystals and Light*, Van Nostrand, New York, 1964.

[10] Born, M. and Wolf, E., *Principles of Optics*, Pergamon Press, New York, 1959.

[11] van der Ziel, A., *Noise*, Prentice-Hall, N.J., 1954.

[12] *American Institute of Physics Handbook*, 2nd ed., McGraw-Hill, New York, 1963.